

Superconductivity in the quasi-two-dimensional Hubbard model

Xin-Zhong Yan

Institute of Physics, Chinese Academy of Sciences, P.O. Box 603, Beijing 100080, China

(Received 8 October 2004; revised manuscript received 30 November 2004; published 29 March 2005)

On the basis of spin-pairing-fluctuation-exchange approximation, we study the superconductivity in the quasi-two-dimensional Hubbard model. The integral equations for the Green's function are self-consistently solved by numerical calculation. Solutions for the order parameter, London penetration depth, density of states, and transition temperature are obtained. Some of the results are compared with the experiments for the cuprate high-temperature superconductors. Numerical techniques are presented in detail. With these techniques, the amount of numerical computations can be greatly reduced.

DOI: 10.1103/PhysRevB.71.104520

PACS number(s): 74.62.-c, 74.20.-z, 74.72.-h, 74.40.+k

I. INTRODUCTION

The Hubbard model has been considered as the basic model to study the mechanism of high-temperature superconductivity in the cuprates.¹ By this model, the spin-fluctuation-exchange between electrons is considered as responsible for the mechanism of high-temperature superconductivity. A number of calculations, taking into account the spin-fluctuation effects, have been devoted to investigating the superconducting properties of the two-dimensional Hubbard models.²⁻¹³

It has been proven that the spin-fluctuation theory can successfully describe a number of properties, including the temperature dependences of the antiferromagnetic correlation length⁹ and the electric resistivity,¹⁴ of the cuprates at high temperatures. However, in most of the calculations on the Hubbard model, the superconducting pairing is treated by the mean-field-like approximation. Such an approximation is not appropriate because the pairing fluctuation is significant in low-dimensional superconducting systems.¹⁵⁻²¹ In fact, the pairing fluctuation can result in new physical consequences. It is believed that the pairing fluctuation is relevant to the pseudogap phenomena^{18,19,22-25} observed in the normal state^{26,27} as well as in the superconducting state²⁸ of the cuprates.

One of the approaches to treating the pairing fluctuation is the ladder-diagram approximation, which has been developed on the quasi-two-dimensional (Q2D) phenomenological model^{18,19} and also on the two-dimensional Hubbard model.^{20,21} By the ladder-diagram approximation, the long-wavelength fluctuation is taken as the predominant contribution. It has been shown that the pairing fluctuations can result in considerable reduction of the transition temperature T_c . According to this approach, T_c vanishes in the absence of interlayer coupling. The reason is that the pairing fluctuation is divergently strong in the two-dimensional system. This is consistent with the Mermin-Wagner-Hohenberg (MWH) theorem.²⁹

In this work, we intend to study the superconductivity in the Q2D Hubbard model. In addition to the spin-fluctuation-exchange (S-FLEX), we take into account the contribution from the pairing fluctuation in the self-energy of the one-particle Green's function. With this spin-pairing-fluctuation-exchange (SP-FLEX) approximation, we investigate the su-

perconductivity in the Q2D Hubbard model. By self-consistently solving the integral equations for the Green's function, we calculate the order parameter, London penetration depth, density of states (DOS), and transition temperature. Some of the results are compared with experiments for the cuprate high-temperature superconductors. In the meanwhile, we also present some numerical techniques in detail in the appendixes, which is necessary for carrying out the numerical solution for the Green's function.

II. FORMALISM

The Q2D Hubbard model defined on a layered cubic lattice is of the following form:³⁰

$$H = - \sum_{\langle \mathbf{ij} \rangle, \alpha} t_{ij} c_{i\alpha}^\dagger c_{j\alpha} + U \sum_{\mathbf{i}} n_{i\uparrow} n_{i\downarrow} - \mu \sum_{\mathbf{i}} (n_{i\uparrow} + n_{i\downarrow}), \quad (1)$$

where t_{ij} denotes the hopping energy of electrons between the lattice sites \mathbf{i} and \mathbf{j} , $c_{i\alpha}^\dagger$ ($c_{i\alpha}$) represents the electron creation (annihilation) operator of spin α at site \mathbf{i} , $n_{i\alpha} = c_{i\alpha}^\dagger c_{i\alpha}$, U is the on-site Coulomb interaction, and μ is the chemical potential. The $\langle \mathbf{ij} \rangle$ sum runs over the nearest-neighbor (NN) sites. In the following, we shall assume $t_{ij} = t$ for the intralayer NN hopping and $t_{ij} = t_z$ for the interlayer NN hopping. A quasi-two-dimensional system is characterized by the condition $t_z/t \ll 1$. Throughout this paper, we use units in which $\hbar = k_B = 1$.

A. Normal state

For simplifying the Feynman diagrams for the Green's function, we present here the approximation scheme for the normal state. The result for the superconducting state can be immediately obtained by adding the anomalous Green's function contributions, and it will be presented in the Sec. II B. The normal Green's function for the electrons is given by

$$G(\mathbf{k}, z_n) = \frac{1}{z_n - \xi_{\mathbf{k}} - \Sigma(\mathbf{k}, z_n)}, \quad (2)$$

where $z_n = i(2n-1)\pi T$ (with T being the temperature of the system) is the imaginary fermionic Matsubara frequency,

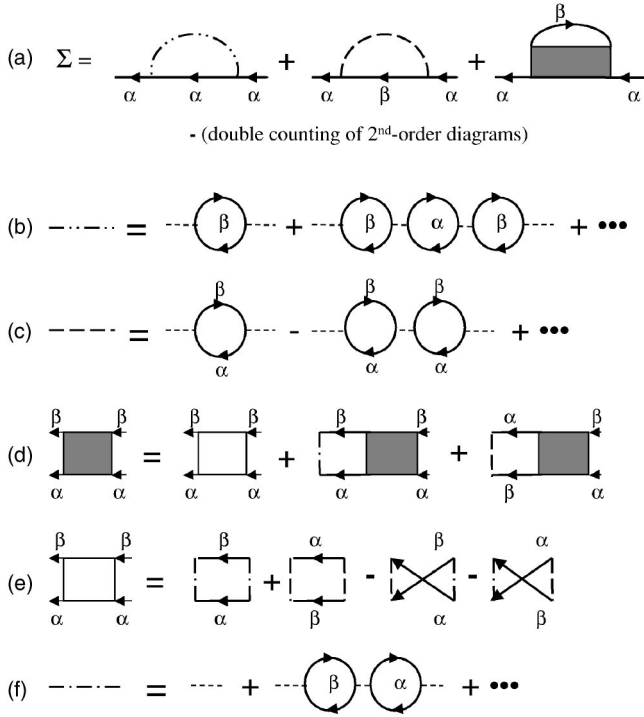


FIG. 1. Approximation scheme for the self-energy. (a) Self-energy for the α -spin electrons. The first term comes from the coupling of the α -spin electrons with the density fluctuation of opposite β -spin electrons. The second term is due to the coupling between transverse spins through their fluctuation. The last term represents the contribution from the pairing fluctuation. (b) Interaction between α -spin electrons due to the density fluctuation of β -spin electrons. (c) Interaction between transverse spins stemming from their fluctuation. (d) Ladder-diagram approximation to the pairing fluctuation. (e) Second order ladder diagrams. (f) Screened Coulomb interaction between electrons of opposite spins.

$\xi_{\mathbf{k}} = -2t(\cos k_x + \cos k_y) - 2t_z \cos k_z - \mu$, and $\Sigma(\mathbf{k}, z_n)$ stands for the electron self-energy. For brevity, occasionally, we use the generalized momentum $k = (\mathbf{k}, z_n)$ in this paper.

Figure 1 shows the approximation scheme for the self-energy. The first two diagrams in Fig. 1(a) are of the well known S-FLEX approximation. These two diagrams can be combined into a single diagram by redefining an effective interaction V_{eff} that is the summation of two interactions given by Figs. 1(b) and 1(c). The expression for V_{eff} is^{5,7,8}

$$V_{\text{eff}}(q) = \frac{3}{2} \frac{U^2 \chi(q)}{1 + U \chi(q)} + \frac{1}{2} \frac{U^2 \chi(q)}{1 - U \chi(q)} - U^2 \chi(q), \quad (3)$$

with

$$\chi(q) = \frac{T}{N} \sum_k G(k+q)G(k). \quad (4)$$

The generalized momentum q stands for (\mathbf{q}, Z_m) , with $Z_m = i2m\pi T$ being the bosonic Matsubara frequency. The first and second terms in the right-hand side of Eq. (3) come, respectively, from the spin and charge fluctuations. The last term eliminates a double counting in the second-order diagrams. Owing to the predominant spin fluctuation, it is

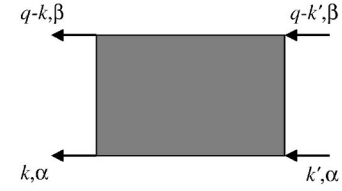


FIG. 2. Ladder diagram representing the propagating of a pair of total momentum q . k' and $q-k'$ are the initial momentum of the α - and β -spin electrons, respectively. After propagating, their momentum changes to k and $q-k$.

named as spin-fluctuation-exchange approximation. The Hartree term has been neglected since it is a constant that can be absorbed in the chemical potential. The third diagram in Fig. 1(a) represents the contribution from the pairing fluctuation. Apart from two interaction sides, the shaded part essentially represents the processes of the electron pair's propagating. Figure 1(d) gives the ladder-diagram approximation for it with the second-order term given by Fig. 1(e). The pairing interaction between two electrons of opposite spins contains two parts, one due to the transverse spin fluctuation (TSF) as given by Fig. 1(c), and another one being the screened Coulomb potential (SCP) given by Fig. 1(f). In the right-hand side of the diagrammatic equation of Fig. 1(e), the first diagram represents the propagating of a pair without changing their spins in the intermediate state, since they interact through SCP during the process. In the second diagram, the intermediate spin configuration is changed because the two electrons interact through the TSF. The third diagram describes the process as the two electrons firstly interact through SCP and then through the mediation of TSF, with a minus factor stemming from the one appearance of TSF. The last diagram is similar to the third one but with an inverse interaction sequence. For brevity, we have dropped all the momentum on these diagrams. The momentum and spins attached to the ladder diagram are illustrated in Fig. 2. For the sake of discussion, we here introduce a notation $L_{\alpha\beta, \beta' \alpha'}(k, q-k; q-k', k')$ for the ladder diagram. In following, we will show that at $T \leq T_c$ the value of the ladder diagram diverges at the long-wavelength limit, $q \rightarrow 0$. Therefore, the pairing fluctuation represented by the ladder diagram gives significant contribution to the self-energy.

To see how the pairing fluctuation takes effect, we consider Fig. 1(d) for the case of a singlet pair of electrons with opposite spins and opposite momentum that is the case of the ladder diagram at the long-wavelength limit. Because of $L_{\alpha\beta, \beta' \alpha'}(k, -k; -k', k') = -L_{\beta\alpha, \alpha' \beta'}(-k, k; -k', k')$, we thereby can combine the last two terms in Fig. 1(d) with an effective pairing interaction V_p defined by Fig. 3(b) and obtain an equation such as Fig. 3(c) but with \approx replaced by $=$ under the ladder-diagram approximation. To solve this equation, we expand the effective pairing interaction in terms of a complete set of basis functions ϕ_n ,

$$V_p(k, k') = \sum_n v_n \phi_n(k) \phi_n(k'). \quad (5)$$

The function ϕ_n satisfies the eigenequation [see Fig. 3(c)],

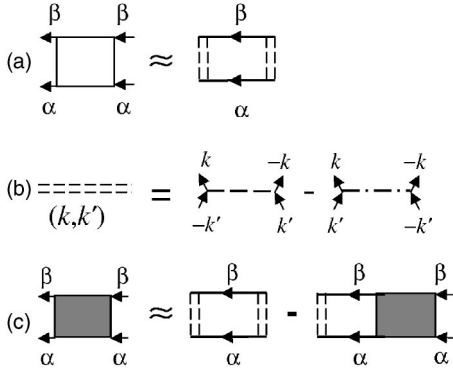


FIG. 3. Approximation to the ladder diagram. (a) Approximate second-order ladder diagram obtained from Fig. 1(e) by neglecting the dependence of the interactions on the total momentum of the pair. (b) Effective pairing interaction. (c) Renormalized diagrammatic equation for the ladder diagram.

$$\frac{T}{N} \sum_{k'} V_P(k, k') G(k') G(-k') \phi_n(k') = \lambda_n \phi_n(k), \quad (6)$$

where N is the total number of lattice sites, and λ_n is the eigenvalue. By so doing, we get^{20,21}

$$L_{\alpha\beta, \beta' \alpha'}(k, -k; -k', k') = - \sum_n \frac{\lambda_n v_n \phi_n(k) \phi_n(k')}{1 - \lambda_n}. \quad (7)$$

At the transition temperature T_c , the largest eigenvalue equals unity, by which the eigenequation (6) then reduces to the gap equation. At the superconducting state, the eigenequation (6) is modified by adding the term of the anomalous Green's function with the largest eigenvalue being unity unchanged. Therefore, at $T \leq T_c$, $L_{\alpha\beta, \beta' \alpha'}(k, -k; -k', k')$ is infinite. It implies that the long-wavelength pairing fluctuation gives significant contribution to the self-energy. On the other hand, as $T \rightarrow T_c$ from the normal state, with the largest eigenvalue of Eq. (6) approaching unity, $L_{\alpha\beta, \beta' \alpha'}(k, -k; -k', k')$ diverges at this limit. Therefore, for the normal state at T close to T_c , the long-wavelength pairing fluctuation is important as well.

From the right-hand side of Eq. (7), we see that, except for the term corresponding to the largest eigenvalue, all other terms are finite. We therefore keep only the most diverging term to simplify the solution of the equation given by Fig. 1(d). That is, we can consider only the pairing of largest eigenvalue.^{20,21,25} For the present case, the largest one is the d -wave pairing. Hereafter, we denote the largest eigenvalue and the corresponding eigenfunction simply as λ_d and $\phi(k)$, respectively, and the coupling constant simply by v .

On observing the above-mentioned fact, we make the approximation in Fig. 1(d) using the pairing interactions of zero total momentum, because near $q=0$ the pairing fluctuation is most significant. We then obtain equations as given by Fig. 3 for determining $L_{\alpha\beta, \beta' \alpha'}(k, q-k; q-k', k')$. Furthermore, by considering only the d -wave pairing that has the largest eigenvalue, the ladder diagram given by Fig. 3(c) reduces to the same one that we previously encountered for

the phenomenological model.¹⁹ Applying the previous result to the present case (see Appendix A), the ladder-diagram summation is obtained as

$$L_{\alpha\beta, \beta\alpha}(k, q-k; q-k', k') = P(q) \phi(k) \phi(k'), \quad (8)$$

with

$$P(q) = \frac{v^2 \Pi(q)}{1 + v \Pi(q)} - v^2 \Pi(q), \quad (9)$$

$$\Pi(q) = - \frac{T}{N} \sum_k \phi^2(k) G(k) G(q-k). \quad (10)$$

In Eq. (9), the last term eliminates all the second-order diagrams since the contribution to the self-energy from the first two diagrams in the right-hand side of the diagrammatic equation of Fig. 1(e) has been taken into account in the S-FLEX approximation, while the other two diagrams are negligible as compared to the infinite ladder-diagram summation. For the self-energy, the final expression is

$$\Sigma(k) = - \frac{T}{N} \sum_q G(k-q) V_{\text{eff}}(q) + \frac{T \phi^2(k)}{N} \sum_q G(q-k) P(q). \quad (11)$$

As we have noted above, the last term in Eq. (11) is corresponding to the previous approximation¹⁹ for the phenomenological model.^{18,19} In that model, however, the interaction is simply a constant d -wave pairing potential, and the hopping energy is proportional to the hole concentration, taking into account the constraint excluding the double occupation. The prohibition of double occupation stems from the t - J model that is the large U limit of the Hubbard model. It is a consequence of strong short-range antiferromagnetic coupling. Under the SP-FLEX approximation scheme for the Hubbard model, however, the antiferromagnetic coupling is taken into account by the first term in Eq. (11). Moreover, for not too large U , the d -wave pairing potential given above varies with the temperature, hole concentration, and U .

A slightly different treatment of the ladder-diagram summation at $q \neq 0$ has been given in Ref. 21. Similarly, the contribution from only the pairing of the largest eigenvalue $\lambda(q)$ was considered. In principle, the eigenvalue $\lambda(q)$ and the eigenfunction should be determined by the corresponding eigenequation at $q \neq 0$. However, it has been found that the eigenfunction depends insensitively on q when q is small. This allows one to determine $\lambda(q)$ using the eigenfunction of $q=0$.²¹ By applying the approximation of the d -wave channel pairing to V_P in the expression for $\lambda(q)$ in Ref. 21, one obtains $\lambda(q) = -v \Pi(q)$ and the same result for the ladder-diagram summation at $q \neq 0$ as given by Eq. (9) except the last unnecessary term.

By the way, we give an expression for the pairing potential. As seen from Figs. 1(c), 1(f), and 3(b), $V_P(k, k')$ equals $V_{1(c)}(k+k') - V_{1(f)}(k-k')$. Since the pairing function $\phi(k)$ can be taken as an even function of k , the pairing potential in Eq. (6) can be thereby written as $V_P(k-k')$. We then have

$$V_P(q) = \frac{3}{2} \frac{U^2 \chi(q)}{1 + U \chi(q)} - \frac{1}{2} \frac{U^2 \chi(q)}{1 - U \chi(q)} - U. \quad (12)$$

Therefore, the left-hand side of Eq. (6) is a convolution of V_P and the rest of it.

In addition, the chemical potential μ should be determined to yield the hole concentration,

$$\delta = -\frac{T}{N} \sum_k [G(k) + G(-k)]. \quad (13)$$

All of the above equations form the closed system that self-consistently determines the Green's function.

B. Superconducting state

For the superconducting state, the above results should be extended to including the contributions from the anomalous Green's function. In the Nambu representation, the Green's function is given by

$$\hat{G}(k) = [z_n - \xi_k \sigma_3 - \hat{\Sigma}(k)]^{-1}, \quad (14)$$

where z_n is understood as $z_n \sigma_0$, and σ is the Pauli matrix. Occasionally, we will use the Pauli components of \hat{G} defined by $\hat{G} = G_0 + G_1 \sigma_1 + G_3 \sigma_3$. Correspondingly, the self-energy is expressed as $\hat{\Sigma} = \Sigma_0 + \Sigma_1 \sigma_1 + \Sigma_3 \sigma_3$ as well. The diagonal element $\Sigma_{11}(k) = \Sigma_0(k) + \Sigma_3(k)$ is given by the same diagram [Fig. 1(a)] except where the effective interaction and the ladder diagram should include the contribution from the anomalous Green's function. The element $\Sigma_{22}(k)$ is obtained by $\Sigma_{22}(k) = -\Sigma_{11}(-k)$. The off-diagonal part Σ_1 is given by the gap equation,

$$\Sigma_1(k) = -\frac{T}{N} \sum_q G_1(k-q) V_P(q). \quad (15)$$

The expressions for V_{eff} and V_P can be obtained as

$$V_{\text{eff}}(q) = \frac{3}{2} \frac{U^2 \chi_-(q)}{1 + U \chi_-(q)} + \frac{1}{2} \frac{U^2 \chi_+(q)}{1 - U \chi_+(q)} - U^2 \chi(q), \quad (16)$$

$$V_P(q) = \frac{3}{2} \frac{U^2 \chi_-(q)}{1 + U \chi_-(q)} - \frac{1}{2} \frac{U^2 \chi_+(q)}{1 - U \chi_+(q)} + U^2 \chi_1(q) - U, \quad (17)$$

with $\chi_{\pm}(q) = \chi(q) \pm \chi_1(q)$, and

$$\chi_1(q) = -\frac{T}{N} \sum_k G_1(k+q) G_1(k). \quad (18)$$

The expression for $\chi(q)$ is the same as Eq. (4) where the Green's function $G(k)$ is understood as $G_{11}(k)$. A simple derivation of these results is presented in Appendix A.

Following the similar analysis as in Sec. II A one can take a corresponding approximation for the pairing fluctuation. In the superconducting case, however, besides the diagonal pair propagating (pairing of particles or holes), attention must be paid to the off diagonal pair propagating as well. The latter is the process in which the initial state is a pair of particles

(holes), while the final state is a pair of holes (particles). Therefore, the pair propagators satisfy a matrix equation. The ladder-diagram approximation with a d -wave channel interaction is given in Appendix A. The function $P(q)$ appearing in Σ_{11} represents the pair propagating. It can be divided into two parts, $P(q) = P_0(q) + P_3(q)$. Their expressions are given by

$$P_0(q) = v[D(q) - 1 - v\Pi_0(q)]/D(q) - v^2\Pi_0(q), \quad (19)$$

$$P_3(q) = v^2\Pi_3(q)[1 - D(q)]/D(q), \quad (20)$$

$$D(q) = [1 + v\Pi_+(q)][1 + v\Pi_-(q)] - v^2\Pi_3^2(q), \quad (21)$$

with $\Pi_{\pm}(q) = \Pi_0(q) \pm \Pi_1(q)$, and

$$\Pi_0(q) = \frac{T}{N} \sum_k \phi^2(k) [G_0(k)G_0(k-q) - G_3(k)G_3(k-q)], \quad (22)$$

$$\Pi_1(q) = \frac{T}{N} \sum_k \phi^2(k) G_1(k)G_1(k-q), \quad (23)$$

$$\Pi_3(q) = \frac{T}{N} \sum_k \phi^2(k) [G_3(k)G_0(k-q) - G_0(k)G_3(k-q)]. \quad (24)$$

The eigenequation for determining the function $\phi(k)$ now is extended to

$$\frac{T}{N} \sum_{k'} V_P(k-k') [G_3^2(k') + G_1^2(k') - G_0^2(k')] \phi(k') = \phi(k), \quad (25)$$

with the largest eigenvalue being unity. This equation is equivalent to Eq. (15) since $\phi(k)$ differs from $\Sigma_1(k)$ by a normalization constant. It also leads to $1 + v\Pi_-(0) = 0$, and thereby $P(q)$ diverges at $q=0$, which means the existence of the Goldstone mode.

In terms of the above functions, the diagonal parts of the self-energy can be expressed as

$$\Sigma_0(k) = -\frac{T}{N} \sum_q G_0(k-q) V_{\text{eff}}(q) - \frac{T\phi^2(k)}{N} \sum_q [G_0(k-q)P_0(q) - G_3(k-q)P_3(q)], \quad (26)$$

$$\Sigma_3(k) = -\frac{T}{N} \sum_q G_3(k-q) V_{\text{eff}}(q) - \frac{T\phi^2(k)}{N} \sum_q [G_0(k-q)P_3(q) - G_3(k-q)P_0(q)]. \quad (27)$$

By using the Pauli component of the Green's function, the expression for Eq. (13) can be simplified as

$$\delta = -\frac{2T}{N} \sum_k G_3(k). \quad (28)$$

So far, we have all the equations for the superconducting case.

C. Q2D approximation

The Green's function $\hat{G}(k)$ and the susceptibilities $\chi(q)$ and $\Pi(q)$ are defined in three-dimensional space. Actually, in case of $t_z/t \ll 1$, they very weakly depend on the z -component variables. However, the dependence on q_z of function $P(q)$ is delicate. Consider the denominator function $D(q)$ at small \mathbf{q} and $Z_m=0$. Since $\Pi(q)$ are even functions of \mathbf{q} , we have

$$D(\mathbf{q},0) \approx c(q_x^2 + q_y^2) + c_z q_z^2, \quad (29)$$

where c and c_z are constants. The q_z^2 term in Eq. (29) comes from the interlayer electron hopping. The ratio c_z/c is much less than unity. If the q_z dependence in $D(q)$ is ignored, the second summations in Eqs. (26) and (27) will be divergent, which implies there will be no superconductivity in the system at finite temperature. This conclusion is consistent with the MWH theorem.²⁹ We therefore need to keep the q_z dependence in the denominators of $P(q)$ at least to the order q_z^2 .

For illustrating our approximation scheme, we firstly consider the case of $Z_m=0$. Since $\Pi_3(\mathbf{q},0)=0$, we have $P_3(\mathbf{q},0)=0$, and

$$P_0 = \frac{v^2}{2} \left[\frac{\Pi_-}{1+v\Pi_-} + \frac{\Pi_+}{1+v\Pi_+} \right] - v^2 \bar{\Pi}_0, \quad (30)$$

where the arguments $(\mathbf{q},0)$ have been dropped for brevity. As has been mentioned in Sec. II B, the first denominator $1+v\Pi_-$ vanishes at $q=0$. Even though the second denominator $1+v\Pi_+$ is finite at $T < T_c$, it is small. Especially, it vanishes too at $T=T_c$. Therefore, we expand both of the denominators to the order q_z^2 ,

$$1+v\Pi_{\pm}(q) \approx 1+v\bar{\Pi}_{\pm}(q) + c_z^{\pm} q_z^2, \quad (31)$$

with

$$\bar{\Pi}_{\pm}(q) = \Pi_{\pm}(q)_{q_z=0}, \quad (32)$$

$$c_z^{\pm} = \frac{v}{2} \frac{d^2}{dq_z^2} \Pi_{\pm}(q)_{q=0}, \quad (33)$$

and use $\bar{\Pi}_{\pm}(q)$ for $\Pi_{\pm}(q)$ in the numerator in Eq. (30). Note that c_z^{\pm} is defined as the derivation in the right-hand side of Eq. (33) at $q=0$ since this is where the q_z dependence is important. To evaluate the constants c_z^{\pm} , we need to take the derivative of the Green's functions $G(q-k)$ with respect to q_z as indicated by Eqs. (22) and (23). By neglecting the q_z dependence of the self-energy, $G(q-k)$ thereby depends on q_z only via ξ_{q-k} . It is expected that such an approximation does not change the physical result so much. To the second order of t_z/t , we obtain¹⁹

$$c_z^{\pm} = \frac{t_z^2 v T}{N} \sum_k \phi^2(k) \left\{ \left[\frac{\partial}{\partial \xi_k} G_3(k) \right]^2 \mp \left[\frac{\partial}{\partial \xi_k} G_1(k) \right]^2 - \left[\frac{\partial}{\partial \xi_k} G_0(k) \right]^2 \right\}, \quad (34)$$

with

$$\frac{\partial}{\partial \xi_k} G_0(k) \approx 2G_0(k)G_3(k),$$

$$\frac{\partial}{\partial \xi_k} G_1(k) \approx 2G_1(k)G_3(k), \quad (35)$$

$$\frac{\partial}{\partial \xi_k} G_3(k) \approx G_0^2(k) - G_1^2(k) + G_3^2(k).$$

With such an approximated $P_0(\mathbf{q},0)$, the integral over q_z in Eqs. (26) and (27) at $Z_m=0$ can be taken immediately by neglecting the q_z dependence in the Green's function. Therefore, instead of $P_0(\mathbf{q},0)$ in Eqs. (26) and (27), we insert in a function defined by

$$P_0^{\text{eff}}(\mathbf{q},0) = \frac{1}{\pi} \int_0^{\pi} dq_z P_0(\mathbf{q},0) = \frac{v^2}{2} [\bar{\Pi}_- f_- + \bar{\Pi}_+ f_+] - v^2 \bar{\Pi}_0, \quad (36)$$

with

$$f_{\pm} = \frac{\gamma^{\pm}(q)}{\pi c_z^{\pm}} \arctan[\pi \gamma^{\pm}(q)], \quad (37)$$

$$\gamma^{\pm}(q) = \left[\frac{c_z^{\pm}}{1+v\bar{\Pi}_{\pm}(q)} \right]^{1/2}, \quad (38)$$

where again, in the last line of Eq. (36), we have dropped the arguments $(\mathbf{q},0)$ for brevity.

We now consider the situation of $Z_m \neq 0$. $D(q)$ is finite in this case. However, to be consistent with the approximation for $P_0(\mathbf{q},0)$, we still keep a small q_z^2 term in the denominator $D(q)$. Though this q_z dependence is negligible at high temperature, it is reasonable in the case of low temperature. According to the expansion by Eq. (31), we expand $D(q)$ as

$$D(q) = \bar{D}(q) + \epsilon(q) q_z^2, \quad (39)$$

with

$$\epsilon(q) = [1+v\bar{\Pi}_+(q)]c_z^- + [1+v\bar{\Pi}_-(q)]c_z^+. \quad (40)$$

To the order q_z^2 , this expansion reduces to the result for the case of $Z_m=0$. Correspondingly, we can define the functions $P_0^{\text{eff}}(q)$ and $P_3^{\text{eff}}(q)$ by taking the integral over q_z . This procedure is equivalent to replacing $1/D(q)$ in Eqs. (22)–(24) with a function $f(q)$ defined by

$$f(q) = \frac{\gamma(q)}{\pi \epsilon(q)} \arctan[\pi \gamma(q)], \quad (41)$$

$$\gamma(q) = \left[\frac{\epsilon(q)}{\bar{D}(q)} \right]^{1/2}. \quad (42)$$

With the functions $P(q)$ in Eqs. (26) and (27) replaced with $P^{\text{eff}}(q)$, the problem of numerically solving the integral equations is then reduced to a two-dimensional one. All of the above are discussed for the case of the superconducting

state. The results for the normal state can be obtained by setting $G_1(k)=0$.

III. NUMERICAL RESULTS

Since the functions $G(k)$, $V_{\text{eff}}(q)$, and $P^{\text{eff}}(q)$ are defined in multidimensional space, they require huge memory storage in the numerical computation process. Especially, the function $P_0^{\text{eff}}(q)$ is singular at $q=0$. Therefore, to carry out the numerical solution, we need to develop a numerical scheme to reduce the amount of computation without losing the accuracy. In Appendix B, we present our scheme for the Matsubara frequency summation. The summation is taken over 57 points, a subset of the frequencies, in a sufficiently large range. The cutoff frequencies are $z_c=(2N_c-1)\pi T$ for the fermions and $Z_c=2(N_c-1)\pi T$ for the bosons, respectively, with $N_c=1017$. For the typical temperature $T/t\sim 0.01$ under consideration, this means $2N_c\pi T/t\sim 64$. For calculating the function $\chi(q)$, beyond this range, the summation over the terms of $n>N_c$ is analytically carried out by using the asymptotic formula of the Green's function,

$$G(\mathbf{k}, z_n) \rightarrow 1/z_n. \quad (43)$$

The error of the summation over the terms of $n>N_c$ is of the order $O(z_c^{-3})$.

The convolutions in the momentum space are carried out with fast Fourier transforms (FFTs) on a 128×128 lattice. For the inverse transform of $V_{\text{eff}}(\mathbf{q}, 0)$ and $P_0^{\text{eff}}(\mathbf{q}, 0)$, i.e., from momentum space to real space, we have to pay special care. At low temperature, $V_{\text{eff}}(\mathbf{q}, 0)$ has strong peaks near $\mathbf{q}=(\pi, \pi)$.⁷ We therefore use a 256×256 mesh in momentum space for the inverse transform. The values of $V_{\text{eff}}(\mathbf{q}, 0)$ for this mesh are obtained by local quadratic polynomial interpolation of the smooth functions $\chi(q)$ given on a 128×128 mesh. On the other hand, the function $P_0^{\text{eff}}(\mathbf{q}, 0)$ has divergently sharp peaks at $\mathbf{q}=0$ and $T\leq T_c$. In Appendix C, we deal with the inverse transform of this function.

The difficulty in solving the eigenvalue problem given by Eq. (6) is that the memory requirement for the coefficient matrix is huge. It is impossible to solve this equation in momentum space. In Appendix C, we rewrite the eigenequation in real space. At high temperature not too close to T_c , Eq. (6) can be solved in real space with a small number of lattice sites in a reduced region. This reduces greatly the amount of numerical calculation work.

The integral equations determining the Green's functions are numerically solved by the iteration method. Once a solution at temperature T is obtained, it is then used as an initial input for the next calculation at temperature $T+\delta T$. A more efficient way is to use an extrapolation from the known solutions at temperatures T_1 and T_2 as the initial input for the next solution at $T_2+\delta T$.

In the present calculation, we set $U/t=5$ and $t_z/t=0.01$. All the results presented in the figures are for these parameters.

A. Eigenvalue λ_d

In Fig. 4, we show the result for the eigenvalue λ_d as function of T at $\delta=0.125$. The S-FLEX result is also pre-

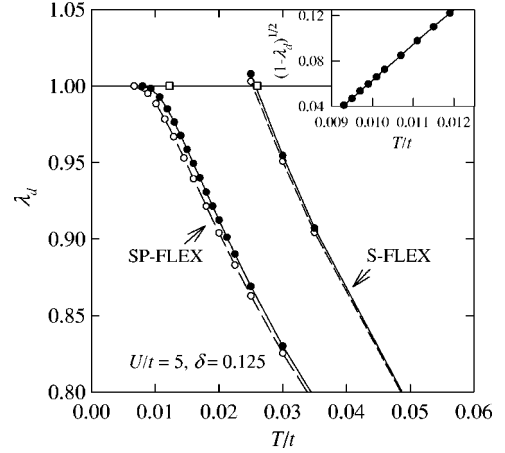


FIG. 4. Eigenvalue λ_d as a function of T at $U/t=5$ and $\delta=0.125$. SP-FLEX is the present approximation. The result of S-FLEX is also depicted for comparison. The solid circles represent the numerical solution to Eq. (6) solved with 49 lattice sites in a reduced region (see Appendix D). The open circles are the results of 25 sites. The squares are the transition points obtained by Eq. (25). The inset shows $(1-\lambda_d)^{1/2}$ of the SP-FLEX approximation as a function of T .

sented for comparison. Due to the pairing fluctuation, the eigenvalue by the present SP-FLEX approximation is considerably reduced from that of the S-FLEX, giving rise to a lower transition temperature. Moreover, there is a distinguishable difference between their behaviors at temperatures close to T_c . By the S-FLEX approximation, we have $d\lambda_d(T)/dT \neq 0$ at $T=T_c$. It means that at $T<T_c$, by keeping no superconducting pairing, the S-FLEX approximation allows a solution of $\lambda_d>1$. In contrast to this feature of the S-FLEX approximation, the solution for λ_d by the SP-FLEX approximation can never get across the line $\lambda_d=1$. At $T\rightarrow T_c$, the pairing fluctuation effect is more pronouncedly with $\lambda_d\rightarrow 1$, which, conversely, suppresses λ_d . As a result, the curve $\lambda_d(T)$ is smoothly connected to the straight line $\lambda_d=1$. That is

$$\left. \frac{d}{dT}\lambda_d(T) \right|_{T_c} = 0. \quad (44)$$

The inset of Fig. 4 shows that $\sqrt{1-\lambda_d}$ varies nearly linearly as $T\rightarrow T_c$, which means $1-\lambda_d \propto (T-T_c)^2$.

A problem then comes in the determination of T_c by $\lambda(T_c)=1$ from the side of the normal state. Because $dT/d\lambda_d=\infty$ at $T=T_c$, a small numerical error in λ_d may result in considerable error in T_c . Therefore, T_c cannot be accurately determined by the function $\lambda_d(T)$. In our numerical calculations, we solved Eq. (6) using two sets of numbers, 25 and 49, respectively, of the lattice sites in the reduced region (see Appendix D). The solid circles in Fig. 4 represent the numerical results of 49 lattice sites, while the open circles are the ones of 25 lattice sites. Close to T_c , the difference between the two results are visible. Even with 49 lattice sites, the transition temperature so determined is not reliable.

The problem can be resolved from the superconducting side. Instead of Eq. (6), we solve Eq. (25). Since the eigen-

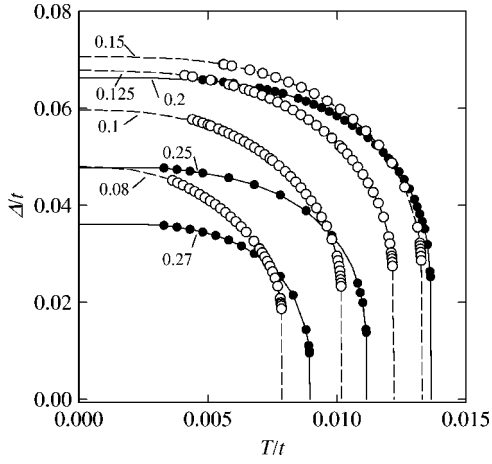


FIG. 5. Order parameter Δ as function of temperature T at various hole concentrations δ . The symbols represent numerical data. The lines are extrapolations. The hole concentrations are indicated by the numbers.

value $\lambda_d=1$ is known at $T \leq T_c$, Eq. (25) can be solved via iteration on the whole lattice. The squares in Fig. 4 denote T_c obtained from the superconducting side for SP-FLEX and S-FLEX, respectively. The numerical solutions for the transition temperatures so determined should be reliable.

B. Order parameter

At low temperature, we have obtained self-consistent solutions in which $\Sigma_1(k)$ is finite. The symmetry of pairing is d wave, $\Sigma_1(\mathbf{k}_x, \mathbf{k}_y, z_n) = -\Sigma_1(\mathbf{k}_y, \mathbf{k}_x, z_n)$. Here, we define the order parameter,

$$\Delta = \Sigma_1(\mathbf{X}, z_1) / Z(\mathbf{X}, z_1) \quad (45)$$

with

$$Z(\mathbf{k}, z_n) = 1 - \Sigma_0(\mathbf{k}, z_n) / z_n \quad (46)$$

and $\mathbf{X} = (\pi, 0)$. The quantity Δ is a measure of the superconducting gap at the Fermi surface near the point \mathbf{X} .^{7,8} Figure 5 shows the order parameter as function of T at various doping concentrations. The symbols represent the numerical data, while the lines are the extrapolations. As seen from Fig. 5, close to T_c , Δ decreases dramatically. (In the numerical calculation, because of this rapid decreasing, to get an iteration converged at temperature $T + \delta T$ with an initial input extrapolated from some other solutions at and close to temperature T , the change δT must be very small. At low doping concentrations, close to T_c , a change of $\delta T/T \sim 10^{-4}$ at most was allowable in the present calculation.) At $T = T_c$, we have $d\Delta(T)/dT = \infty$. Because of this divergence, T_c can be accurately determined by $\Delta = 0$.

On the other hand, at low temperature, $\Delta(T)$ should be flat. We then can obtain the value $\Delta_0 \equiv \Delta(0)$ by extrapolation. In Fig. 6, we show the ratio $2\Delta_0/k_B T_c$ at various doping concentrations. At the underdoping regime, the ratio is about an order of 10. It decreases with the doping concentration. This ratio is considered as a characterization of the coupling strength of the system. The low-doping regime corresponds

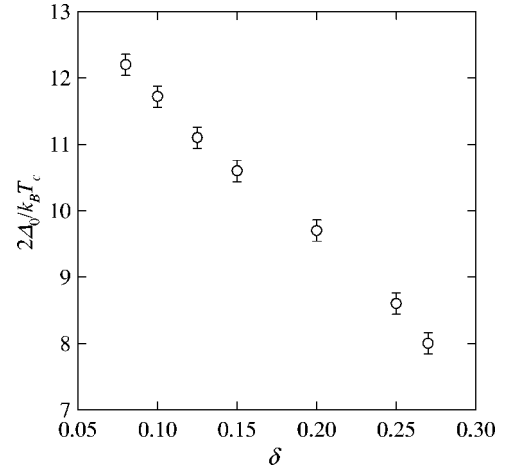


FIG. 6. Ratio $2\Delta_0/k_B T_c$ at various hole concentrations δ .

to strong coupling. While increasing the doping concentration, the coupling becomes weak.

C. Phase diagram

As mentioned in Sec. III B, the transition temperature T_c is determined by $\Delta(T_c) = 0$, which gives an accurate solution for T_c . The present SP-FLEX result at $U/t=5$ (solid circles) for the boundary of superconducting phase in the $T_c - \delta$ phase diagram is depicted in Fig. 7. All the solid circles are obtained by numerical solutions. The S-FLEX result (open circles) is also shown for comparison. Clearly, due to the pairing fluctuation, T_c is considerably reduced from that of the S-FLEX approximation. The reduction is more significant at lower hole doping where T_c decreases with decreasing δ . On the other hand, at large δ , the pairing fluctuation is less pronounced. This is consistent with the previous

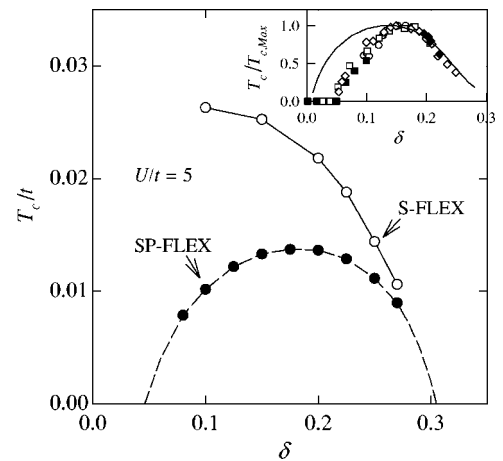


FIG. 7. Transition temperature T_c as function of hole concentration δ . The solid circles and open circles are obtained at $U/t=5$ by the SP-FLEX and S-FLEX calculations, respectively. The dashed line is an extrapolation of the numerical result. In the inset, the symbols denote the experimental results for the cuprate high-temperature superconductors (Ref. 31) while the solid line is the previous result (Ref.19) for the phenomenological model.

conclusion.¹⁹ The results of the previous calculation on the phenomenological model (with coupling constant $J/t=0.2$)¹⁹ and the experiments³¹ for the cuprate high-temperature superconductors are exhibited in the inset of Fig. 7 for comparison. The behavior of the previous result at small hole doping clearly differs from the experiment and the present calculation. It may stem from the crude treatment of the short-range antiferromagnetic coupling by the phenomenological model. In contrast to the previous result, the present calculation gives a reasonable description of the experiment at small hole doping.

The dashed line in Fig. 7 is an extrapolation of the numerical result. Unlike the previous case for the phenomenological model,¹⁹ the extrapolation gives a nonzero minimum hole concentration δ_m , very close to 0.05, of the phase boundary. Again, this seems to reasonably reflect the feature of the experimental result. The largest transition temperature $T_{c,\max}$ obtained by SP-FLEX is about $0.0137t$ at $\delta=0.175$. Using $t \approx 0.6$ eV,^{18,19} we have $T_{c,\max} \approx 95$ K.

To see why the pairing fluctuation results in the reduction of T_c , we analyze the self-energy given by Eq. (11) [which is the same as that given by Eqs. (26) and (27) at $T=T_c$] with $P(q)$ replaced by $P^{\text{eff}}(q)$. At $Z_m \approx 0$, since $V_{\text{eff}}(q)$ and $P^{\text{eff}}(q)$ have strong negative peaks, respectively, at $\mathbf{q} \approx \mathbf{Q} \equiv (\pi, \pi)$ and $\mathbf{q}=0$, we here make a crude approximation (for the sake of illustration) for the self-energy,

$$\begin{aligned} \Sigma(k) \approx & -G(\mathbf{k}-\mathbf{Q}, z_n) \left[\frac{T}{N} \sum_{q \sim \mathbf{Q}} V_{\text{eff}}(q) \right] + G(\mathbf{k}, -z_n) \\ & \times \left[\frac{T\phi^2(k)}{N} \sum_{q \sim 0} P^{\text{eff}}(q) \right]. \end{aligned} \quad (47)$$

The summations in the square brackets give rise to two negative quantities. At small δ , $\mu \approx 0$, we have $G(\mathbf{k}-\mathbf{Q}, z_n) \approx -G(\mathbf{k}, -z_n)$. Taking this fact into account, we get $\Sigma(k) \approx -G(\mathbf{k}, -z_n)\Gamma_k^2$, with $\Gamma_k^2 = a_1 + a_2\phi^2(k)$, where a_1 and a_2 are two positive constants. Substituting the result into Eq. (2), one obtains

$$G(\mathbf{k}, z_n) \approx \frac{z_n + \xi_k}{2\Gamma_k^2} \left(1 - \sqrt{1 + \frac{4\Gamma_k^2}{\xi_k^2 - z_n^2}} \right). \quad (48)$$

Applying these results to Eq. (6), we see that the factor $G(k)G(-k)$ is reduced and so is T_c .

Physically, the quantity

$$a_2 = -\frac{T}{N} \sum_{q \sim 0} P^{\text{eff}}(q)$$

is a measure of the density of pairs at their excited states. Since the function $P^{\text{eff}}(q)$ is given in terms of $\bar{\Pi}(q)$, we analyze $\bar{\Pi}(q) = \Pi(q)|_{q_z=0}$, especially at $q=0$. From Eq. (10), we see that the quantity $\Pi(0)$ comes predominately from the summation over the points close to the Fermi surface in momentum space. At smaller δ , the Fermi surface of the Hubbard model is larger and so is the number of the pairs at their fluctuating states. Therefore, the reduction on T_c is larger at smaller δ .

The form of the Green's function given by Eq. (48) implies that there exists a pseudogap in the energy spectrum of the electrons.^{19,32} Consider the spectral function,

$$\begin{aligned} A(\mathbf{k}, E) &= -\frac{1}{\pi} \text{Im}G(\mathbf{k}, E + i0^+) \\ &= \frac{E + \xi_k}{2\pi\Gamma_k^2} \sqrt{\frac{\xi_k^2 + 4\Gamma_k^2 - E^2}{E^2 - \xi_k^2}}, \end{aligned}$$

which is nonzero only for $E^2 - 4\Gamma_k^2 < \xi_k^2 < E^2$. The noninteraction delta-function peak becomes a square root singularity. Because of the constraint, the area of the \mathbf{k} space of $A(\mathbf{k}, E) \neq 0$ decreases as $E \rightarrow 0$, resulting in a suppression of the density of states. Especially, the density of states vanishes at $E=0$ (for $\mu=0$) since the area becomes zero and the singularity disappears there.

On observing the function Γ_k^2 , we note that the pseudogap stems from the spin and pairing fluctuations. Even at $T=0$, the pseudogap remains in the superconducting state because the spin fluctuation (owing to which the superconductivity takes place) and the pairing fluctuation (coming from the Goldstone mode¹⁹) exist. This may explain the recent experiment.²⁸

D. Density of states

The density of states is defined by

$$\rho(E) = -\frac{1}{\pi N} \sum_{\mathbf{k}} \text{Im}G_{11}(\mathbf{k}, E + i0^+). \quad (49)$$

The Green's function needs to be analytically continued from the imaginary Matsubara frequency to the real frequency. In terms of an effective self-energy $\tilde{\Sigma}(k)$ defined by

$$\tilde{\Sigma}(k) = \Sigma_0(k) + \Sigma_3(k) + \frac{\Sigma_1^2(k)}{z_n - \xi_k - \Sigma_0(k) + \Sigma_3(k)}, \quad (50)$$

the Green's function $G_{11}(k)$ is written as

$$G_{11}(k) = \frac{1}{z_n - \xi_k - \tilde{\Sigma}(k)}. \quad (51)$$

Using the Padé approximation,³³ we have obtained the analytical continuation for the effective self-energy $\tilde{\Sigma}(k)$.

The results for the density of states at $\delta=0.125$ at various temperatures are depicted in Fig. 8. At low temperature, the width of the gap is nearly constant. Below T_c , a peak-dip-hump (PDH) structure is clearly seen above the Fermi energy. The positions of the peak and dip are about Δ and 3Δ , respectively. Such a phenomenon has been observed in the cuprates experiments and has been explained by model calculations.^{34,35} The PDH stems from a coupling between the electrons and a collective mode of energy about 2Δ . Below T_c , the superconducting gap opens with the maximum of 2Δ appearing in the region near the points $(\pm\pi, 0)$ and $(0, \pm\pi)$ in the Brillouin zone. The collective spin-fluctuation mode of energy 2Δ and momentum \mathbf{Q} can then exist in the system. An electron of energy 3Δ can transit to a state of

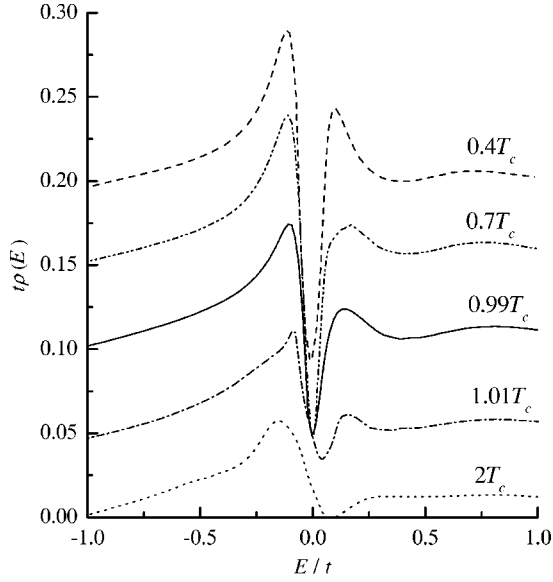


FIG. 8. Density of states $\rho(E)$ at $\delta=0.125$ at various temperatures. For clarity, the y axes for the results of $0.7T_c$ and $0.4T_c$ have been offset upwards by 0.05 and 0.1, respectively. For $1.01T_c$ and $2T_c$, the offsets are downwards 0.05 and 0.1, respectively.

energy Δ (at which the DOS has a peak) by exciting the collective mode and losing energy 2Δ . Effectively, the lifetime of the electrons of energy 3Δ is short, and thereby the dip appears in the DOS. In the fluctuation-exchange (FLEX) scheme, such a collective mode is described by the effective interaction V_{eff} that is self-consistently determined by the present calculation.

On the other hand, above T_c , there still remains a pseudogap in the DOS. While increasing the temperature, the minimum moves to high energy. As stated in Sec. III C, the pseudogap comes from both of the spin and pairing fluctuations. At higher temperature, the pairing fluctuation is less important. The electron states \mathbf{k} and $\mathbf{k}+\mathbf{Q}$ couple with each other mainly through the spin fluctuations. Especially, the degeneracy of those states at the magnetic zone surface is lifted and the weights shift away, resulting in a reduction in the DOS at the corresponding energy.

E. London penetration depth

In this section, we study the magnetic penetration depth. The London penetration depth λ_L in x direction is given via

$$\lambda_L^{-2} = \frac{4\pi n e^2}{m^* c^2} + \frac{4\pi}{c^2} C(q) \Big|_{q=0}, \quad (52)$$

with $C(q)$ the y -component current-current correlation function defined by

$$C(\mathbf{q}, \tau - \tau') = -\langle T_\tau J_y(\mathbf{q}, \tau) J_y(-\mathbf{q}, \tau') \rangle / N, \quad (53)$$

where $\langle \dots \rangle$ means a statistical average T_τ is the imaginary time τ ordering operator, and J_y is the y -component current operator,

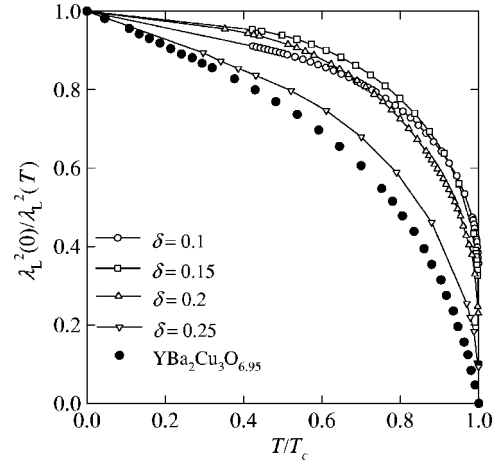


FIG. 9. Quantity $\lambda_L^2(0)/\lambda_L^2(T)$ as a function of temperature T at various doping concentrations δ . The solid circles denote the experimental results for a -axis penetration depth of $\text{YBa}_2\text{Cu}_3\text{O}_{6.95}$.

$$\mathbf{J}(\mathbf{q}) = -e \sum_{\mathbf{k}\alpha} \nabla_{\mathbf{k}} \xi_{\mathbf{k}} c_{\mathbf{k}-\mathbf{q}/2\alpha}^\dagger c_{\mathbf{k}+\mathbf{q}/2\alpha}.$$

In Eq. (52), n and m^* are the number density and the effective mass of electrons, respectively. By using the Ward identity for the current vertex, the quantity $C_0 = C(q)|_{q=0}$ can be written as

$$C_0 = \frac{e^2 T}{N} \sum_{\mathbf{k}} [G_{11}^2(\mathbf{k}) + G_{12}^2(\mathbf{k})] \nabla_{\mathbf{k}} \xi_{\mathbf{k}} \cdot \mathbf{v}_{\mathbf{k}}, \quad (54)$$

with $\mathbf{v}_{\mathbf{k}} = \nabla_{\mathbf{k}} [\xi_{\mathbf{k}} + \tilde{\Sigma}_{11}(\mathbf{k})]$. By noting the following equations:

$$G_{11}^2(\mathbf{k}) \nabla_{\mathbf{k}} [\xi_{\mathbf{k}} + \tilde{\Sigma}(k)] = \nabla_{\mathbf{k}} G_{11}(\mathbf{k}),$$

$$\frac{T}{N} \sum_{\mathbf{k}} \nabla_{\mathbf{k}} \xi_{\mathbf{k}} \cdot \nabla_{\mathbf{k}} G_{11}(\mathbf{k}) = -\frac{n}{m^*},$$

we get the expression for λ_L^{-2} ,

$$\lambda_L^{-2} = \frac{4\pi e^2 T}{c^2 N} \sum_{\mathbf{k}} [G_{12}^2(\mathbf{k}) \mathbf{v}_{\mathbf{k}} - G_{11}^2(\mathbf{k}) \mathbf{u}_{\mathbf{k}}] \cdot \nabla_{\mathbf{k}} \xi_{\mathbf{k}}, \quad (55)$$

with

$$\mathbf{u}_{\mathbf{k}} = \nabla_{\mathbf{k}} \frac{\Sigma_1^2(k)}{z_n - \xi_{\mathbf{k}} - \Sigma_0(k) + \Sigma_3(k)}.$$

By Eq. (55), λ_L^{-2} vanishes identically at and above T_c .

Shown in Fig. 9 are the results for the quantity $\lambda_L^{-2}(T)$ as a function of temperature T at various doping concentrations. The experimental result for the a -axis penetration depth of $\text{YBa}_2\text{Cu}_3\text{O}_{6.95}$ is also presented for comparison.³⁶ It is well known that $\lambda_L^{-2}(T)$ under d -wave pairing symmetry varies linearly with T at low T . Using this property, we infer the value $\lambda_L^{-2}(0)$ from the extrapolation of the known results at finite temperatures. We then get the zero-temperature superfluid density n_s . Figure 10 shows the relationship between T_c and n_s at a number of doping concentrations. This result resembles the experimental observation by Uemura *et al.*³⁷ They have found a universal linear relation between T_c and

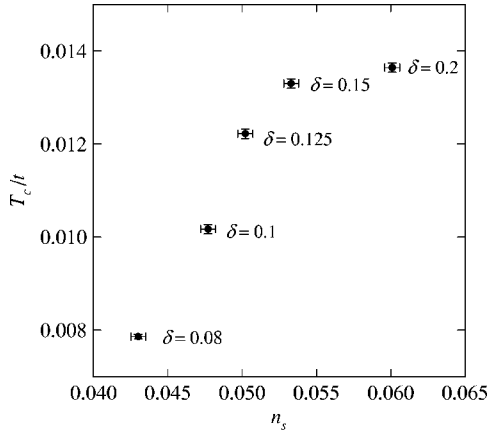


FIG. 10. T_c vs n_s at various doping concentrations δ .

n_s/m^* at underdoping regime. This behavior cannot be explained by the BCS theory, nor by the S-FLEX scheme in which T_c and n_s do not decrease with δ decreasing.

In the mean-field theory, the electron pairs are all considered as being in the Bose-Einstein condensate below T_c . Since the pairing interaction (stemming from the spin-fluctuation exchange) is stronger at smaller doping concentrations, more electron pairs are produced in the condensate. This leads to higher T_c and a larger superfluid density. In contrast to the mean-field theory, in the SP-FLEX scheme, the electron pairs are allowed to occupy their excited states. At low temperature, those collective modes are the most available excited states. Even at the ground state, there remains the zero-point motion for the collective modes. So, only a part of the pairs stay in the condensate. As stated earlier, the pairing fluctuation is stronger at smaller δ , resulting in lower T_c and lower n_s .

IV. SUMMARY

In summary, we have investigated the d -wave superconductivity in the quasi-two-dimensional repulsive Hubbard model. Both of the spin and pairing fluctuations are taken into account in the self-energy. We have self-consistently solved the integral equations for the Green's function. The present calculations reflect a number of features of the experimental results for the cuprate high-temperature superconductors. The calculated boundary of the superconducting phase shows a parabolic-like shape, reasonably describing the experiments. The peak-dip-hump structure in the density of states is naturally reproduced. In addition, the present calculations give reasonable explanations for the temperature dependence of the penetration depth and the relationship between T_c and the superfluid density.

The pairing fluctuation implies that an amount of pairs occupy their excited states. This fluctuation effect leads to the reduction of the condensation of the pairs and, thereby, the transition temperature.

ACKNOWLEDGMENTS

The author thanks Professor C. S. Ting for useful discussions on the related problems. This work was supported by

Natural Science Foundation of China under Grant No. 10174092 and by Department of Science and Technology of China under Grant No. G1999064509.

APPENDIX A

Considering the convenience for readers, we here present simple derivations of the effective interaction V_{eff} , the pairing potential V_p , and the ladder-diagram approximation for the pair propagators for the superconducting state.

Firstly, we consider the extension of Fig. 1(b). The interaction $V_b(q)$ between α -spin electrons can be written as

$$V_b(q) = U^2 \tilde{\chi}^{\beta\beta}(q), \quad (\text{A1})$$

where $\tilde{\chi}^{\beta\beta}(q)$ is the density-density response function between the opposite β -spin electrons. Generally, the function $\tilde{\chi}^{\alpha\alpha'}$ in the imaginary time τ space is defined as

$$\tilde{\chi}^{\alpha\alpha'}(\mathbf{q}, \tau - \tau') = -\langle T_\tau n_\alpha(\mathbf{q}, \tau) n_{\alpha'}(-\mathbf{q}, \tau') \rangle / N, \quad (\text{A2})$$

where $n_\alpha(\mathbf{q}, \tau)$ is the density operator of α -spin electrons. In the Matsubara-frequency space, the Dyson equation for $\tilde{\chi}^{\alpha\alpha'}(q)$ reads

$$\tilde{\chi}^{\alpha\alpha'}(q) = \chi^{\alpha\alpha'}(q) + \sum_\gamma \chi^{\alpha\gamma}(q) U \tilde{\chi}^{-\gamma\alpha'}(q), \quad (\text{A3})$$

where the γ summation runs over the up and down spins, and χ are the irreducible response functions. Under the ring approximation, from Eq. (A2), $\chi^{\alpha\alpha}(q)$ is obtained as the same as given by Eq. (4) where the Green's function $G(k)$ is understood as $G_{11}(k)$. $\chi^{\beta\beta}(q)$ is equal to $\chi^{\alpha\alpha}(q)$ because of the equality of the up and down spin electrons. For $\alpha \neq \beta$, we have $\chi^{\alpha\beta}(q) = \chi^{\beta\alpha}(q) \equiv \chi_1(q)$ as given by Eq. (18). Solving Eq. (A3) and substituting the result into Eq. (A1), we have

$$V_b(q) = \frac{U}{2} \left[\frac{1}{1 - U\chi_+(q)} - \frac{1}{1 + U\chi_-(q)} \right], \quad (\text{A4})$$

with $\chi_\pm(q) = \chi(q) \pm \chi_1(q)$.

Secondly, for the interaction between transverse spins corresponding to Fig. 1(c), we write

$$V_c(q) = U^2 \tilde{\chi}^{+-}(q), \quad (\text{A5})$$

with $\tilde{\chi}^{+-}(q)$ being the response function between transverse spins defined by

$$\tilde{\chi}^{+-}(\mathbf{q}, \tau - \tau') = -\langle T_\tau S^+(\mathbf{q}, \tau) S(\mathbf{q}, \tau') \rangle / N, \quad (\text{A6})$$

and $S^+(\mathbf{q}, \tau) = \sum_{\mathbf{k}} c_{\mathbf{k}\uparrow}^\dagger(\tau) c_{\mathbf{k}+\mathbf{q}\downarrow}(\tau)$. From Eq. (A6), the irreducible function can be obtained as $\chi^{+-}(q) = \chi_-(q)$. Since $\tilde{\chi}^{+-}(q)$ satisfies the Dyson equation, $\tilde{\chi}^{+-}(q) = \chi_-(q) - \chi_-(q) U \tilde{\chi}^{+-}(q)$, we have

$$V_c(q) = \frac{U^2 \chi_-(q)}{1 + U\chi_-(q)}. \quad (\text{A7})$$

With the above results, for the effective interaction $V_{\text{eff}}(q) = V_b(q) + V_c(q) - U^2 \chi(q)$, we get the expression as given by Eq. (16).

Analogously, the interaction corresponding to Fig. 1(f) can be written as

$$V_f(q) = U + U^2 \tilde{\chi}^{\alpha\beta}(q). \quad (\text{A8})$$

From Eq. (A3), we have

$$\tilde{\chi}^{\alpha\beta}(q) = \frac{1}{2} \left[\frac{\chi_+(q)}{1 - U\chi_+(q)} - \frac{\chi_-(q)}{1 + U\chi_-(q)} \right]. \quad (\text{A9})$$

The result for the pairing potential $V_P(q) = V_c(q) - V_f(q) + U^2\chi_1(q)$ is then obtained as given by Eq. (17). Again, the term $U^2\chi_1(q)$ eliminates a second-order double counting.

Finally, the function $P(q)$ appearing in the element $\Sigma_{11}(k)$ of the self-energy can be expressed as

$$P(q) = v^2 [\tilde{\Pi}_{11}(q) - \Pi_{11}(q)], \quad (\text{A10})$$

where $\tilde{\Pi}_{11}(q)$ is the pair-pair response function, and $\Pi_{11}(q)$ is the irreducible part (or the pair susceptibility, which eliminates the second-order double counting). The function $\tilde{\Pi}_{\mu\nu}(\mathbf{q}, \tau - \tau')$ is defined as

$$\tilde{\Pi}_{\mu\nu}(\mathbf{q}, \tau - \tau') = - \langle T_\tau p_\mu(\mathbf{q}, \tau) p_\nu^\dagger(\mathbf{q}, \tau') \rangle / N, \quad (\text{A11})$$

with $\mu, \nu = 1, 2$, $p_1(\mathbf{q}) = \sum_{\mathbf{k}} \phi(k) c_{\mathbf{q}-\mathbf{k}\downarrow} c_{\mathbf{k}\uparrow}$, and $p_2(\mathbf{q}) = \sum_{\mathbf{k}} \phi(k) c_{\mathbf{k}\uparrow}^\dagger c_{-\mathbf{k}\downarrow}^\dagger$. Strictly speaking, p_1 and p_2 are not the Schrödinger operators since $\phi(k)$ depends on the Matsubara frequency. Here, we formally regard them as only depending on the momentum. At the end, we extend the result to include the frequency dependence. (Alternatively, one can draw the Feynman diagram from the beginning. The final result is the same.) From Eq. (A11), the expressions for the irreducible susceptibilities can be obtained as Eqs. (22)–(24).

The Dyson equation for $\tilde{\Pi}_{\mu\nu}$ in matrix form is

$$\hat{\tilde{\Pi}}(q) = \hat{\Pi}(q) - v \hat{\Pi}(q) \hat{\tilde{\Pi}}(q). \quad (\text{A12})$$

The diagonal parts of the Pauli components of the matrix $\hat{P}(q) = v^2 [\hat{\tilde{\Pi}}(q) - \hat{\Pi}(q)]$ can be expressed as Eqs. (19) and (20).

APPENDIX B

In this appendix, we intend to develop an algorithm for the approximate summation of a series. It is analogous to Simpson's integral method. Firstly, we consider the following summation:

$$S(n_0, n_2) = \sum_{n=n_0}^{n_2} f(n), \quad (\text{B1})$$

where $n_2 = n_0 + 2h$ with h an integer. Suppose $f(x)$ is a smooth function over the range $n_0 < x < n_2$. We then expand $f(n)$ as

$$f(n) \approx f(n_0) + c_1(n - n_0) + c_2(n - n_0)^2, \quad (\text{B2})$$

where c_1 and c_2 are constants. With the given values $f_j \equiv f(n_0 + jh)$, for $j=0, 1$, and 2 , the constants can be expressed as

$$c_1 = (-3f_0 + 4f_1 - f_2)/2h,$$

$$c_2 = (f_0 - 2f_1 + f_2)/2h^2.$$

Substituting Eq. (B2) into Eq. (B1), we get

$$S(n_0, n_2) \approx \frac{h}{6} (2 + 3y + y^2)(f_0 + f_2) + \frac{h}{3} (4 - y^2)f_1, \quad (\text{B3})$$

with $y = 1/h$. Therefore, the summation over the entire range $[n_0, n_2]$ can be obtained approximately with only three values, f_0, f_1 , and f_2 , given. At $y \rightarrow 0$, Eq. (B3) reduces to the Simpson rule. With the approximation (B2), we even can carry out a summation over a part of the range $[n_0, n_2]$. For more general uses, for $n_0 \leq m \leq n_2$, we have

$$S(n_0, m) \approx Af_0 + Bf_1 + Cf_2, \quad (\text{B4})$$

with

$$A = h(y + z)[1 - 3z/4 + z(y + 2z)/12],$$

$$B = h(y + z)z[1 - (y + 2z)/6],$$

$$C = -h(y + z)z[1 - (y + 2z)/3]/4,$$

and $z = (m - n_0)/h$.

Now, we consider the summation $S(1, \infty)$. When $f(n)$ decreases fast at $n \rightarrow \infty$, $S(1, \infty)$ can be obtained approximately over a finite range with the cutoff number sufficiently large. We may divide this range into several blocks within each of which $f(x)$ can be regarded as a smooth function and thereby the above algorithm can be applied. At most cases, $f(n)$ may vary fast at small n . Therefore, the stride h should be shorter at smaller n . Here, we introduce a point-selection scheme. Consider L successively connected blocks. The selected points divide each block into $M-1 (\geq 2)$ equal-spaced segments; each block contains M points. The stride (the length of the segment) in the l th block is $h_l = h^{l-1}$ with h a constant integer number. By such a scheme, the number corresponding to the j th point in the l th block is

$$n_{[j,l]} = \left(j - 1 + \frac{M-1}{h-1} \right) h^{l-1} - \frac{M-h}{h-1}, \quad (\text{B5})$$

for $j=1, 2, \dots, M$ and $l=1, 2, \dots, L$. The cutoff number is $N_c = n_{[M,L]}$. By repeatedly using the above summation algorithm, one can get approximately

$$S(1, \infty) \approx \sum_p w_p f(n_p), \quad (\text{B6})$$

where p runs over the $L(M-1)+1$ selected points, and w_p is the weight at point $p \equiv [j, l]$. Note that because of $n_{[M,l]} = n_{[1, l+1]}$, such points should be counted once in the summation. The point-selection scheme uniquely determines the weights. If $M \geq 5$ is an odd number, applying the above summation algorithm, we get

$$w_{[1,1]} = 1,$$

$$w_{[j,l]} = (4h^{l-1} - h^{1-l})/3 \quad \text{for } j=2, 4, \dots, M-1,$$

$$w_{[j,l]} = (2h^{l-1} + h^{1-l})/3 \quad \text{for } j=3, 5, \dots, M-2,$$

$$w_{[M,1]} = (2h + 3 + h^{-1})/6,$$

$$w_{[M,l]} = w_{[1,l+1]} = h^l(1 + h^{-1})/3 + (1 + h)h^{-l}/6$$

for $l = 2, \dots, L - 1$,

$$w_{[M,L]} = h^{L-1}/3 + 1/2 + h^{1-L}/6.$$

To justify the above summation algorithm, we here give an example. Consider the summation,

$$S = \sum_{j=1}^{\infty} \frac{2}{4j^2 - 1} = 1. \quad (\text{B7})$$

Applying the above algorithm with $h=2$, $L=7$, and $M=9$, we have

$$S_{\text{sum}} = \sum_p \frac{2w_p}{4n_p^2 - 1} = 0.999\ 52. \quad (\text{B8})$$

The relative error is $(S_{\text{sum}} - S)/S = -4.8 \times 10^{-4}$. Note that the term under the summation in Eq. (B7) decreases by $1/2j^2$ at large j . If one uses the known result,

$$\sum_{j=1}^{\infty} j^{-2} = \pi^2/6,$$

the accuracy of the summation can be improved much better. Instead of Eq. (B8), we calculate the following summation:

$$S_{\text{sum}} = \sum_p w_p \left(\frac{2}{4n_p^2 - 1} - \frac{1}{2n_p^2} \right) + \pi^2/12. \quad (\text{B9})$$

With such an arrangement, the value of the brackets in the p summation decreases by $O(n_p^{-4})$ at large n_p . This summation gives a very accurate result $S_{\text{sum}} = 1.000\ 000\ 15$, with a small relative error of only 1.5×10^{-7} .

In some cases, with the given points $n_{[j,l]}$ selected in advance, we need to calculate the summations, $S(1, n)$, with $n_{[j_0, l_c]} \leq n < n_{[j_0+1, l_c]}$ and $l_c \leq L$. In these cases, because the summation over a range needs three points at least, the terminate number $n_c \equiv n_{[j_c, l_c]}$ is then determined as follows:

$$j_c = \begin{cases} 3, & \text{if } j_0 = 1 \\ j_0 + 1, & \text{otherwise.} \end{cases}$$

Since the summation $S(1, n)$ can be expressed as $S(1, n) = S(1, n_{[1, l_c]} - 1) + S(n_{[1, l_c]}, n)$, the weights at the points $n_p < n_{[1, l_c]}$ as tabulated above are unchanged, while at the points $n_{[j, l_c]}$, for $j = 1, \dots, j_c$, w_p should be reevaluated according to the algorithm as given by Eq. (B4).

For testing the accuracy of the algorithm for summations of finite terms, we consider the following example:

$$S_n = \sum_{j=1}^n \frac{2}{4j^2 - 1} = \frac{2n}{2n + 1}. \quad (\text{B10})$$

With the $[h, L, M] = [2, 7, 9]$ scheme, the summation is approximated as

TABLE I. Ratio of S_{sum} given by Eq. (A11) and $S_n = 2n/(2n + 1)$ at various n . RE represents the relative error.

n	S_{sum}/S_n	RE
5	1.000000	0.0
10	1.000047	0.000047
50	1.000012	0.000012
100	1.000013	0.000013
500	1.000013	0.000013

$$S_{\text{sum}} = \sum_p \frac{2w_p^n}{4n_p^2 - 1}, \quad (\text{B11})$$

where we use superscript n indicating the n dependence of the weights. The results for S_{sum}/S_n are given in Table I. The relative error, $(S_{\text{sum}} - S_n)/S_n$, is less than 10^{-4} .

Finally, we give the expression for the susceptibility χ . Since it is even for Z_m , we only consider the case of $m \geq 0$. In real space, it is given by

$$\begin{aligned} \chi(r, Z_m) &= T \sum_{n=-\infty}^{\infty} G(r, z_n) G(r, z_n + Z_m) \\ &= T \left\{ 2 \sum_{n=1}^{\infty} G(r, z_n) G(r, z_n + Z_m) \right. \\ &\quad \left. + 2 \sum_{n=1}^{[m/2]} G(r, z_n) G(r, z_n - Z_m) \right. \\ &\quad \left. + G(r, z_{\bar{n}}) G(r, -z_{\bar{n}}) \Big|_{\bar{n}=(m+1)/2} \text{ if } m \text{ is odd} \right\}, \\ &= T \left\{ 2 \sum_p w_p G(r, z_{n_p}) G(r, z_{n_p} + Z_m) \right. \\ &\quad \left. + 2 \sum_p w_p^{[m/2]} G(r, z_{n_p}) G(r, z_{n_p} - Z_m) \right. \\ &\quad \left. + G(r, z_{\bar{n}}) G(r, -z_{\bar{n}}) \Big|_{\bar{n}=(m+1)/2} \text{ if } m \text{ is odd} \right\} + \delta\chi(r, Z_m), \end{aligned}$$

where $[m/2]$ is the integer part of $m/2$, and the last term is given by

$$\delta\chi(r, Z_m) = 2T \sum_{n=N_c+1}^{\infty} G(r, z_n) G(r, z_n + Z_m).$$

Because of $G(r, z_n) \rightarrow \delta_{r0}/z_n$ at $n \rightarrow \infty$, we have

$$\delta\chi(r, Z_m) = \begin{cases} -\frac{\delta_{r0}}{m\pi^2 T} \sum_{n=N_c+1}^{N_c+m} \frac{1}{2n-1} & \text{if } m > 0 \\ -\frac{2\delta_{r0}}{\pi^2 T} \left[\frac{\pi^2}{8} - \sum_{n=1}^{N_c} \frac{1}{(2n-1)^2} \right] & \text{if } m = 0. \end{cases}$$

Note that $G(r, z_n - Z_m) = G^*(r, Z_m - z_n)$. Therefore, the Green's function at negative Matsubara frequency can be determined from its complex counterpart at the positive frequency. For a

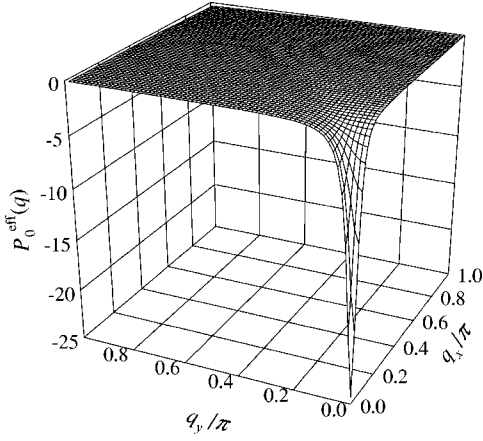


FIG. 11. Function $P_0^{\text{eff}}(q)$ in unit of $2t$ at $Z_m=0$, $\delta=0.125$, $U/t=5$, and $T/t=0.0124$.

given point-selection scheme, $G(r, z_{n_p})$ is known. Those values at $Z_m \pm z_n$ can be evaluated by interpolation, or $G(r, z_n + Z_m) \approx \delta_{r0}/(z_n + Z_m)$ if $n+m > N_c$.

APPENDIX C

In this appendix, we discuss the problem of inverse Fourier transform of $P_0^{\text{eff}}(\mathbf{q}, 0)$. A typical result for $P_0^{\text{eff}}(\mathbf{q}, 0)$ is shown in Fig. 11. This function behaves as $P_0^{\text{eff}}(\mathbf{q}, 0) \propto 1/\sqrt{a^2 + q^2}$ (with $q^2 = q_x^2 + q_y^2$) at $q \rightarrow 0$. The constant a vanishes at $T \leq T_c$. Even at $T > T_c$ but close to T_c , a is very small. Physically, it means that the pairing fluctuation is defined in a long range in real space. Especially, at $T \leq T_c$, the range is infinite. Therefore, its primary form is not suitable for a numerical inverse Fourier transform on a finite lattice.

The function $P_0^{\text{eff}}(\mathbf{q}, 0)$ can be divided into the ‘‘singular’’ part $c/\sqrt{a^2 + q^2}$ (with c a constant) and the regular one. There is no problem in the inverse Fourier transform for the latter one. For the singular part, the task is to calculate the integral,

$$F(j_x, j_y) = \int_0^\pi dq_x \int_0^\pi dq_y \frac{\cos(q_x j_x) \cos(q_y j_y)}{\sqrt{a^2 + q^2}}, \quad (\text{C1})$$

where j_x and j_y are the coordinates of a lattice site. Repeatedly integrating by part, we get

$$\begin{aligned} F(j_x, j_y) = & -j_y^2 \int_0^\pi dq_x \int_0^\pi dq_y f_1(q) \cos(q_x j_x) \cos(q_y j_y) \\ & + (-1)^{j_y} \int_0^\pi dq_x f_2(q_x) \cos(q_x j_x) \\ & - j_x \int_0^\pi dq_x f_3(q_x) \sin(q_x j_x) - (-1)^{j_x} f_3(\pi), \quad (\text{C2}) \end{aligned}$$

with

$$\begin{aligned} f_1(q) &= q_y \ln(q_y + \sqrt{a^2 + q^2}) - \sqrt{a^2 + q^2}, \\ f_2(q_x) &= \ln(\pi + \sqrt{a^2 + \pi^2 + q_x^2}), \end{aligned}$$

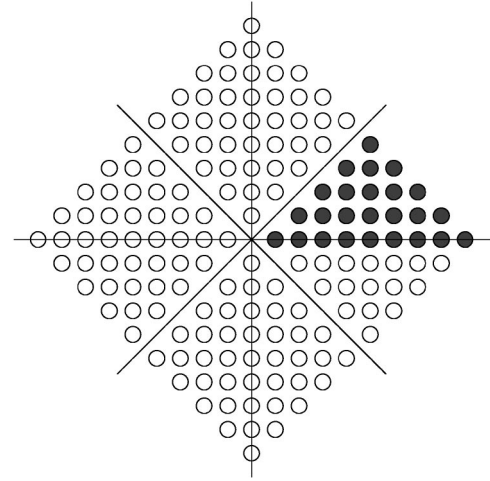


FIG. 12. Sketch of the lattice sites used for solving Eq. (D9). Solid circles show the reduced region.

$$f_3(q_x) = q_x (\ln \sqrt{a^2 + q_x^2} - 1) + a \arctan\left(\frac{q_x}{a}\right).$$

By this way, all f are regular functions.

However, because the large factors j_y^2 and j_x at long distances, we need to carry out the inverse Fourier transforms in Eq. (C2) with high accuracy. The numerical method of the fast Fourier transforms amounts to applying the trapezoidal rule to the integral in Eq. (C2). One may use a very dense mesh in the Brillouin zone for the transforms. But, this is uneconomical in the present numerical process since such transforms need to be repeatedly performed. In fact, errors in the numerical integration stem mainly from the rapid oscillation behavior in the integrand. Here, we present our scheme for these integrals in Eq. (C2). Essentially, we need to deal with the following integrals:

$$F_c(j) = \int_0^\pi dq f(q) \cos(qj), \quad (\text{C3})$$

$$F_s(j) = \int_0^\pi dq f(q) \sin(qj), \quad (\text{C4})$$

where $f(q)$ is a regular and smooth function over $(0, \pi)$.

Firstly, we consider the simple case,

$$I(q_1, q_3) \equiv \int_{q_1}^{q_3} dq f(q) \cos(qj), \quad (\text{C5})$$

where (q_1, q_3) is a small range. The middle point is q_2 . Within this range, $f(q)$ can be expressed as

$$f(q) \approx a_1 + a_2(q - q_1) + a_3(q - q_1)^2. \quad (\text{C6})$$

The constants a are determined by the values $f_j \equiv f(q_j)$,

$$a_1 = f_1,$$

$$a_2 = (-3f_1 + 4f_2 - f_3)/2h,$$

$$a_3 = (f_1 - 2f_2 + f_3)/2h^2,$$

where $h = q_2 - q_1$. Now, repeatedly integrating Eq. (C5) by part and using Eq. (C6), we obtain

$$I(q_1, q_3) = C_1 \cos(q_1 j) + C_3 \cos(q_3 j) + S_1 \sin(q_1 j) + S_3 \sin(q_3 j), \quad (C7)$$

with

$$C_1 = (3f_1 - 4f_2 + f_3)h/2x^2,$$

$$C_3 = (f_1 - 4f_2 + 3f_3)h/2x^2,$$

$$S_1 = [f_3 - 2f_2 - (x^2 - 1)f_1]h/x^3,$$

$$S_3 = [(x^2 - 1)f_3 + 2f_2 - f_1]h/x^3,$$

and $x = jh$. It is expected that the result given by Eq. (C7) is more accurate than the trapezoidal rule.

Now, dividing the range $(0, \pi)$ into $2M$ equally spaced pieces, we have

$$F_c(j) = \sum_{k=1}^M I(q_{2k-1}, q_{2k+1}), \quad (C8)$$

with $q_k = (k-1)h$ and $q_{2M+1} = \pi$. Using the result as given by Eq. (C7), we get

$$F_c(j) = 2w_1(x) \left[2 \sum_{k=2}^M f_{2k-1} \cos(q_{2k-1} j) + f_1 + (-1)^j f_{2M+1} \right] + 4w_2(x) \sum_{k=1}^M f_{2k} \cos(q_{2k} j), \quad (C9)$$

where the functions w_1 and w_2 are given by

$$w_1(x) = \frac{h}{4x^2} \left[3 - \frac{2 \sin(2x)}{x} + \cos(2x) \right],$$

$$w_2(x) = \frac{h}{x^2} \left(\frac{\sin x}{x} - \cos x \right).$$

Define a new discrete function,

$$g_k = (-1)^k f_k \quad \text{for } k = 1, \dots, 2M+1.$$

With this definition, Eq. (C9) can be rewritten as

$$F_c(j) = w_1(x) \{C_j[f] - C_j[g]\} + w_2(x) \{C_j[f] + C_j[g]\}, \quad (C10)$$

where $C_j[f]$ is the cosine Fourier transform of function f defined by

$$C_j[f] = 2 \sum_{k=2}^{N-1} f_k \cos(q_k j) + f_1 + (-1)^j f_N$$

with $N = 2M + 1$. Therefore, the function $F_c(j)$ can be evaluated by the FFT via Eq. (C10).

Similarly, one can get

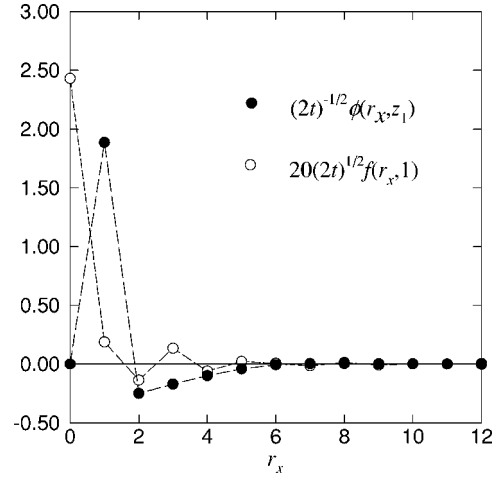


FIG. 13. Functions $f(r_x, 1)$ and $\phi(r_x, z_1)$ at $r_y=0$, $\delta=0.125$, $U/t=5$, and $T/t=0.0124$. The dashed lines are for the eyes.

$$F_s(j) = w_1(x) \{S_j[f] - S_j[g]\} + w_2(x) \{S_j[f] + S_j[g]\} + \frac{h}{x} \left[1 + \frac{\sin(2x)}{2x} - \frac{1 - \cos(2x)}{x^2} \right] [f_1 - (-1)^j f_N], \quad (C11)$$

where $S_j[f]$ is the sine Fourier transform of function f defined by

$$S_j[f] = 2 \sum_{k=2}^{N-1} f_k \sin(q_k j).$$

APPENDIX D

In this appendix, we rewrite the eigenequation (6) in a form more convenient for the numerical calculation. We intend to solve the equation in real space in order to get rid of the prohibitive storage requirement for the coefficient matrix in momentum space.

We can apply the frequency-summation algorithm just developed in Appendix B to the present case, so reducing the memory size. However, to solve the eigenequation in momentum space still requires tremendous memory size. In some cases, fortunately, the pairing function is short ranged in real space. We therefore solve the equation in real space. To transform Eq. (6) into real space, one needs to maintain the matrix of the coefficients to be symmetrical. In the following, we present the transformation procedure.

(a) Define functions $f(\mathbf{k}, n_p)$ and $\psi(\mathbf{k}, n_p)$ as

$$f(\mathbf{k}, n_p) \equiv \sqrt{T w_p} G(\mathbf{k}, z_{n_p}) G(-\mathbf{k}, -z_{n_p}), \quad (D1)$$

$$\psi(\mathbf{k}, n_p) \equiv f(\mathbf{k}, n_p) \phi(\mathbf{k}, z_{n_p}), \quad (D2)$$

where w_p is the weight at frequency z_{n_p} as introduced in Appendix B. In real space, Eq. (6) is transformed to

$$\sum_{\mathbf{r}' p'} A(\mathbf{r}, n_p; \mathbf{r}', n_{p'}) \psi(\mathbf{r}', n_{p'}) = \lambda \psi(\mathbf{r}, n_p), \quad (D3)$$

with

$$A(\mathbf{r}, n_p; \mathbf{r}', n_{p'}) = \sum_{\mathbf{R}} f(\mathbf{r} - \mathbf{R}, n_p) W(\mathbf{R}, n_p, n_{p'}) f(\mathbf{R} - \mathbf{r}', n_{p'}), \quad (\text{D4})$$

and

$$W(\mathbf{R}, n_p, n_{p'}) = V_p(\mathbf{R}, z_{n_p} - z_{n_{p'}}) + V_p(\mathbf{R}, z_{n_p} + z_{n_{p'}}). \quad (\text{D5})$$

(b) Furthermore, because of the lattice symmetry, we need only to consider the lattice sites $[r]$ of $0 \leq r_y < r_x$. Those lattice sites of $r_x = r_y$ are excluded since the d -wave pairing is under consideration. Define

$$y(\mathbf{r}, n) = 2 \sqrt{\frac{2}{d_r}} \psi(\mathbf{r}, n) \quad (\text{D6})$$

$$F(\mathbf{r}, \mathbf{R}, n) = \frac{1}{\sqrt{d_r d_R}} \sum_g s_g f(g\mathbf{r} - \mathbf{R}, n) \quad (\text{D7})$$

where $d_r = 1 + \delta_{r,0}$, the g summation runs over the operations of group C_{4v} , $s_g = \pm 1$ is the sign factor of the d -wave function $\phi(\mathbf{r}, z_n)$ under the operation g , and $g\mathbf{r}$ denotes a site coming from \mathbf{r} , operated by g . Accordingly, define the new matrix,

$$M(\mathbf{r}, n_p; \mathbf{r}', n_{p'}) = \sum_{[\mathbf{R}]} F(\mathbf{r}, \mathbf{R}, n_p) W(\mathbf{R}, n_p, n_{p'}) F(\mathbf{r}', \mathbf{R}, n_{p'}), \quad (\text{D8})$$

where again $[\mathbf{R}]$ summation runs over those lattice sites of $0 \leq R_y < R_x$. By so doing, the eigenequation reads,

$$\sum_{[\mathbf{r}']_{p'}} M(\mathbf{r}, n_p; \mathbf{r}', n_{p'}) y(\mathbf{r}', n_{p'}) = \lambda y(\mathbf{r}, n_p). \quad (\text{D9})$$

A sketch of the lattice sites is shown in Fig. 12. The reduced region $[r]$ is taken as the solid circles, which are suitable for the description of d -wave pairing. In our numerical calculation, the total number of sites of $[r]$ is $N_r = 49$. The normalization condition for $y(\mathbf{r}, n_p)$ is

$$\sum_{[\mathbf{r}]_p} y^2(\mathbf{r}, n_p) = 1. \quad (\text{D10})$$

By this condition, the coupling constant v is given as $v = \lambda/2$. Shown in Fig. 13 are the typical results for $f(r_x, 1)$ and $\phi(r_x, z_1)$. Clearly, they are short-ranged functions. In passing, we compare the sizes of the matrices of the coefficients required for solving the eigenequation, respectively, in real and momentum spaces. The dimension of matrix M in Eq. (D8) is $(N_r M_0) \times (N_r M_0) = 2793 \times 2793$, where $M_0 = 57$ is the number of the selected Matsubara frequency. However, in momentum space with a 128×128 mesh, even making use of the lattice symmetry, the dimension is $(N_k M_0) \times (N_k M_0) = 118\,560 \times 118\,560$, where $N_k = 32 \times 65$ is the number of momentum \mathbf{k} with $0 \leq k_y < k_x \leq \pi$.

-
- ¹P. W. Anderson, *Science* **235**, 1196 (1987).
²Z. Y. Weng, T. K. Lee, and C. S. Ting, *Phys. Rev. B* **38**, 6561 (1988).
³J. R. Schrieffer, X. G. Wen, and S. C. Zhang, *Phys. Rev. Lett.* **60**, 944 (1988); *Phys. Rev. B* **39**, 11 663 (1989).
⁴G. Vignal and K. S. Singwei, *Phys. Rev. B* **39**, 2956 (1989).
⁵N. E. Bickers, D. J. Scalapino, and S. R. White, *Phys. Rev. Lett.* **62**, 961 (1989).
⁶P. Monthoux and D. Pines, *Phys. Rev. Lett.* **69**, 961 (1992); *Phys. Rev. B* **49**, 4261 (1994); P. Monthoux, A. V. Balatsky, and D. Pines, *ibid.* **46**, 14 803 (1992).
⁷C. H. Pao and N. E. Bickers, *Phys. Rev. Lett.* **72**, 1870 (1994); *Phys. Rev. B* **49**, 1586 (1994); **51**, 16 310 (1995).
⁸P. Monthoux and D. J. Scalapino, *Phys. Rev. Lett.* **72**, 1874 (1994).
⁹T. Dahm and L. Tewordt, *Phys. Rev. B* **52**, 1297 (1995).
¹⁰R. Putz, R. Preuss, A. Muramatsu, and W. Hanke, *Phys. Rev. B* **53**, 5133 (1996).
¹¹S. Koikegami, S. Fujimoto, and K. Yamada, *J. Phys. Soc. Jpn.* **66**, 1438 (1997).
¹²T. Takimoto and T. Moriya, *J. Phys. Soc. Jpn.* **66**, 2459 (1997); **67**, 3570 (1998).
¹³H. Kontani, K. Kanki, and K. Ueda, *Phys. Rev. B* **59**, 14 723 (1999).
¹⁴T. Moriya, Y. Takahashi, and K. Ueda, *J. Phys. Soc. Jpn.* **59**, 2905 (1990); K. Ueda, T. Moriya, and Y. Takahashi, *J. Phys. Chem. Solids* **53**, 1515 (1992).
¹⁵V. J. Emery and S. A. Kivelson, *Nature (London)* **374**, 434 (1995).
¹⁶E. Babaev and H. Kleinert, *Phys. Rev. B* **59**, 12 083 (1999).
¹⁷Z. Tesanovic, O. Vafek, and M. Franz, *Phys. Rev. B* **65**, 180511 (R) (2002).
¹⁸B. Jankó, J. Maly, and K. Levin, *Phys. Rev. B* **56**, R11 407 (1997); I. Kosztin, Q. J. Chen, Y. J. Kao, and K. Levin, *ibid.* **61**, 11 662 (2000); Q. Chen, I. Kosztin, B. Jankó, and K. Levin, *Phys. Rev. Lett.* **81**, 4708 (1998); Q. Chen, I. Kosztin, and K. Levin, *ibid.* **85**, 2801 (2000).
¹⁹X. Z. Yan, *Int. J. Mod. Phys. B* **17**, 319 (2003); X. Z. Yan, *J. Phys.: Condens. Matter* **15**, L319 (2003).
²⁰T. Dahm, D. Manske, and L. Tewordt, *Phys. Rev. B* **55**, 15 274 (1997).
²¹Y. Yanase and K. Yamada, *J. Phys. Soc. Jpn.* **70**, 1659 (2000).
²²C. A. R. Sá de Melo, M. Randeria, and J. R. Engelbrecht, *Phys. Rev. Lett.* **71**, 3202 (1993); *Phys. Rev. B* **55**, 15 153 (1997).
²³J. R. Engelbrecht, A. Nazarenko, M. Randeria, and E. Dagotto, *Phys. Rev. B* **57**, 13 406 (1998); T. Hotta, M. Mayr, and E. Dagotto, *ibid.* **60**, 13 085 (1999).
²⁴B. Kyung, S. Allen, and A.-M. S. Tremblay, *Phys. Rev. B* **64**, 075116 (2001).
²⁵H. Kontani, *Phys. Rev. Lett.* **89**, 237003 (2002).
²⁶G. V. M. Williams, J. L. Tallon, R. Michalak, and R. Dupree, *Phys. Rev. B* **54**, R6909 (1996).

- ²⁷Ch. Renner, B. Revaz, J. -Y. Genoud, K. Kadowaki, and Ø. Fischer, Phys. Rev. Lett. **80**, 149 (1998); V. M. Krasnov, A. Yurgens, D. Winkler, P. Delsing, and T. Claeson, Phys. Rev. Lett. **84**, 5860 (2000); M. Suzuki and T. Watanabe, *ibid.* **85**, 4787 (2000).
- ²⁸J. L. Tallon, J. W. Loram, J. R. Cooper, C. Panagopoulos, and C. Bernhard, Phys. Rev. B **68**, 180501(R) (2003).
- ²⁹N. D. Mermin and H. Wagner, Phys. Rev. **17**, 1133 (1966); P. C. Hohenberg, Phys. Rev. **158**, 383 (1967).
- ³⁰J. Hubbard, Proc. R. Soc. London **276**, 238 (1963); **277**, 237 (1963).
- ³¹J. L. Tallon, C. Bernhard, H. Shaked, R. L. Hitterman, and J. D. Jorgensen, Phys. Rev. B **51**, R12 911 (1995), and references therein.
- ³²J. J. Deisz, D. W. Hess, and J. W. Serene, Phys. Rev. Lett. **76**, 1312 (1996).
- ³³H. J. Vidberg and J. W. Serene, J. Low Temp. Phys. **29**, 179 (1977).
- ³⁴Z. X. Shen and J. R. Schrieffer, Phys. Rev. Lett. **78**, 1771 (1997); M. Eschrig and M. R. Norman, *ibid.* **85**, 3261 (2000); A. Abanov and A. V. Chubukov, Phys. Rev. B **61**, R9241 (2000).
- ³⁵Y. DeWilde, N. Miyakawa, P. Guptasarma, M. Iavarone, L. Ozyuzer, J. F. Zasadzinski, P. Romano, D. G. Hinks, C. Kendziora, G. W. Crabtree, and K. E. Gray, Phys. Rev. Lett. **80**, 153 (1998).
- ³⁶A. Hosseini, S. Kamal, D. A. Bonn, R. Liang, and W. N. Hardy, Phys. Rev. Lett. **81**, 1298 (1998).
- ³⁷Y. J. Uemura, G. M. Luke, B. J. Sternlieb, J. H. Brewer, J. F. Carolan, W. N. Hardy, R. Kadono, J. R. Kempton, R. F. Kiefl, S. R. Kreitzman, P. Mulhern, T. M. Riseman, D. Li. Williams, B. X. Yang, S. Uchida, H. Takagi, J. Gopalakrishnan, A. W. Sleight, M. A. Subramanian, C. L. Chien, M. Z. Cieplak, Gang Xiao, V. Y. Lee, B. W. Statt, C. E. Stronach, W. J. Kossler, and X. H. Yu, Phys. Rev. Lett. **62**, 2317 (1989).